TAYLOR, W.R. A new froth pump for improved pumping of viscous thickener underflow. *The 6th International Platinum Conference, 'Platinum–Metal for the Future',* The Southern African Institute of Mining and Metallurgy, 2014.

A new froth pump for improved pumping of viscous thickener underflow

W.R. TAYLOR
Weir Minerals Africa (Pty) Ltd

The mining and mineral extraction industry generates a wide range of slurries. During the initial stages of size reduction in the mill, the ore is mixed with water to form a slurry and then transferred throughout the process by means of slurry pumping.

An essential part of most beneficiating processes is that of slurry thickening, which is done to increase the density of the slurry product for specific needs (better mineral recoveries, lower operating costs, reduced water handling). The continuous concentration of fine particles can easily affect the slurry rheology, resulting in very viscous or even non-Newtonian type slurries.

Thickeners are used to increase the solids concentration by sedimentation. Solids settle over the entire bottom of the thickener tank, while blades or rakes assist with the compaction of the settled particles to ultimately produce thickened underflow slurry. The solids in the thickener move continuously downwards and then inwards towards the underflow outlet as a thickened pulp.

Pumping of very viscous or non-Newtonian underflow slurries has traditionally presented challenges to end-users utilizing conventional centrifugal slurry pumps.

A new horizontal centrifugal froth pump with a patented inlet and flow inducer impeller design has been developed by Weir Minerals to help overcome the performance problems associated with frothy slurries. However, this design proved exceptional for difficult-to-pump viscous and non-Newtonian thickener underflow slurries.

From test work carried out in a phosphate concentrate thickener underflow application, the new patented Warman® AHF™ heavy-duty froth pump fitted with the Hi Seal® dry gland expeller configuration demonstrated improved centrifugal pumping performance and extended the boundary for viscous slurry transportation.

Thickened phosphate rock concentrate at densities above 1990 kg/m^3 is successfully transferred with the new froth pump technology.

This paper discusses and presents the results of the on-site test work, and demonstrates the fundamental design differences between the conventional horizontal centrifugal slurry pump and the new heavy-duty horizontal centrifugal froth pump technology.

Introduction

Conventional centrifugal slurry pumps are the most economical means of moving high volumes of slurries. These centrifugal slurry pumps are often installed in applications where viscous and non-Newtonian slurries are required to be pumped over short distances, and where the system pressures fall within their rated pump casing pressures.

Generally, the higher the viscosity of the slurry, the more resistance it presents to flow and consequently the more difficult it is to pump. Certain viscous and non-Newtonian slurries may be too difficult to pump with centrifugal pumps, therefore understanding the properties of the particular slurry remains essential. Although it is important to quantify the shape and size of the slurry particles, a thorough understanding of the rheology is probably the most important aspect to consider prior to any centrifugal pump selection. Analysing these slurries and predicting how they perform when pumped remains a complex task, especially when dealing with non-Newtonian rheological fluids, whose behaviour is time-dependent. Due to their high concentration of solids and chemical and physical properties, these slurries do not flow nearly as well as water, and this contributes to a number of problems at the pump inlet. The effect of these difficult slurries on the performance of conventional centrifugal slurry pumps has for the greater part, always been problematic to users. However, the technological developments of the new froth pump – the large inlet and patented flow inducer impeller – seemed favourable for pumping viscous and non-Newtonian type slurries (Burgess, 2004).

This froth pump technology was officially launched in South Africa in 2009, and in 2011 the first Warman® 6F-AHF™ froth pump was installed and tested on a rougher concentrate froth transfer application at the Foskor phosphate mine in Phalaborwa. The results of this trial demonstrated significant froth pumping improvements (Taylor, 2013). This paved the way to initiate test work on thickener underflow slurry applications.

Terminology and classification of slurries

Slurry types range from fine slurries containing sub-micrometre particle sizes to coarse slurries with particle sizes exceeding well beyond the 400 μm size fraction. These can be classified into settling slurries and non-settling slurries according to the settling behaviour of the particles comprising the slurry mixture. Slurries that are centrifugally pumped can be characterized as either Newtonian or non-Newtonian on the basis of their rheology.

The Newtonian theory forms the starting point for many non-Newtonian pipe flow models. Newtonian and non-Newtonian slurries can exhibit laminar, transitional, and turbulent flow behaviour.

Newtonian theory

In cases of Newtonian liquids, the shear stress is proportional to the velocity gradient. This simply implies that Newton's law of viscosity relates shear stress (τ) to the velocity gradient, also known as the rate of shear strain, or simply the rate of shear (du/dy), using a constant of proportionality known as the dynamic or absolute viscosity (μ) of the fluid. To complement the above, if a fluid is in motion, shear stresses are developed when particles of the fluid move relative to each other.

For successive layers of flow over a flat plate, the velocity of the fluid (u) will vary from layer to layer as distance from the plate (y) increases. Figure 1 indicates the variations in fluid velocity with distance from a flat plate (Burgess, 2004).

It can therefore be stated that for Newtonian liquids, the slope of the shear stress versus shear rate is constant while the velocity is constant at a given pressure and temperature.

Figure 2 reinforces this discussion by demonstrating that at zero shear rate, the shear stress is equal to zero and thus the rheogram of a Newtonian fluid is a straight line that passes through the origin. Any imposed shear stress causes the fluid to flow (Wilson *et al*., 2006).

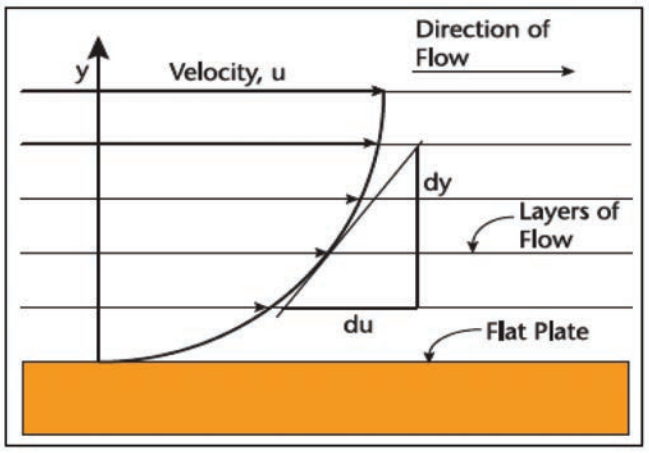


Figure 1.Variation in fluid velocity with distance from a flat plate (Burgess, 2004)

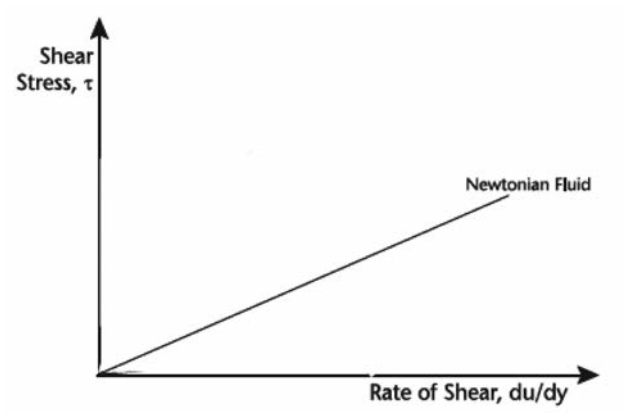


Figure 2. Shear stress versus shear rate – Newtonian rheogram (Wilson *et al*., 2006)

Non-Newtonian theory

Non-Newtonian fluids are either homogeneous or heterogeneous with variable compositions, as per the following categories.

- Bingham plastic
- Pseudoplastic
- Dilatant fluid
- Thixotropic fluid
- Rheopectic fluid.

It is important to note that a non-Newtonian fluid or mixture has one or more of the following characteristics:

- A curvilinear rheogram
- A rheogram that does not pass through the origin (threshold)
- A rheogram that varies with time *i.e*. is dependent on shear history.

This serves to help explain why the shear stress versus shear rate rheograms could be curved and could have positive values at their origins (Burgess, 2004).

Figure 3 represents the complex rheograms for most of the abovementioned non-Newtonian categories.

From Figure 3 it can be seen that due to constant dynamic

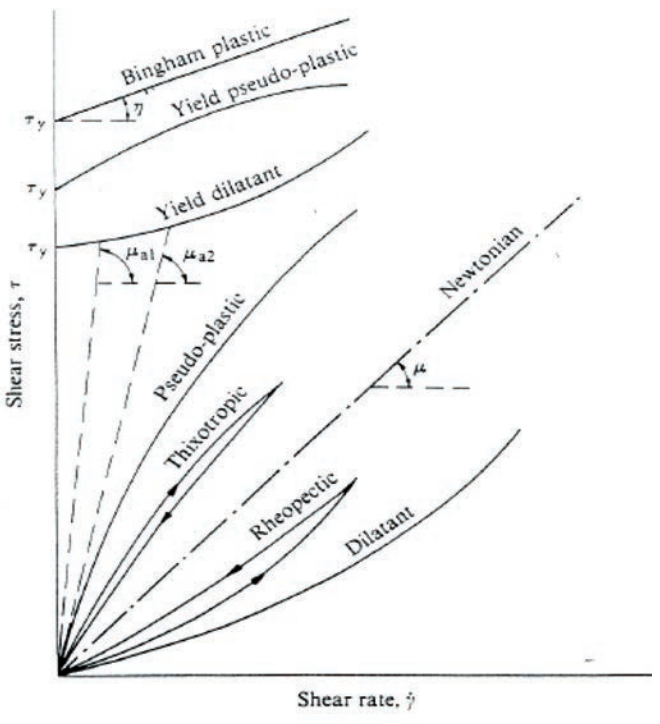


Figure 3. Representation of most non-Newtonian rheograms (Burgess, 2004)

viscosity, Newtonian and Bingham plastic fluids display linear rheograms.

In contrast to the Newtonian and Bingham plastic rheograms, shear rate-dependent viscosities produce curvilinear rheograms for the pseudoplastic and dilatant fluids. It is further noted that dilatant, Newtonian, and pseudoplastic liquids have zero shear stress at a zero shear rate, confirming that they do not require a minimum shear stress to start flowing. If the concentration of slurry particles continually decreases, the non-Newtonian slurry could become a Newtonian fluid. However, if the concentration of a non-Newtonian slurry continually increases, the consistency (apparent viscosity) increases proportionally until a critical concentration is reached, after which even small changes in the concentration will contribute to significant changes in the viscosity (Lozhechnikova, 2011).

Figure 4 indicates that as the concentration of the slurry increases, the yield stress and the coefficient of rigidity increase rapidly (Burgess, 2004).

The coefficient of rigidity is the measure of a material's resistance to shearing stress, equal to the shearing stress divided by the resultant angle of deformation expressed in radians (TheFreeDictionary.com, 2014).

Effect of viscous slurries on pump performance

Slurries can be characterized as either Newtonian or non-Newtonian, based on their rheology. Non-Newtonian slurries can be further categorized as homogeneous or heterogeneous, and demonstrate complex rheograms. Discussions on the protracted rheograms expand on their typical rheological behaviours to assist in a better understanding of their complex microstructures, which exhibit variable relationships between shear stress and shear rate.

As many homogeneous slurries show shear thinning or shear thickening behaviour, it remains fundamentally important that the design characteristics of the centrifugal slurry pump (with much emphasis on the pump inlet and the pump impeller design) will be able to accomplish the optimum intent. In this context, the optimum intent would be to ensure that once the slurry has passed through the pump, it is thoroughly sheared so as to reach its asymptotic rheologic behaviour (Wilson *et al*., 2006).

For the pumping of difficult to flow time-behaviour slurries, the above statement is of paramount importance to the optimal operation of the entire pumping system.

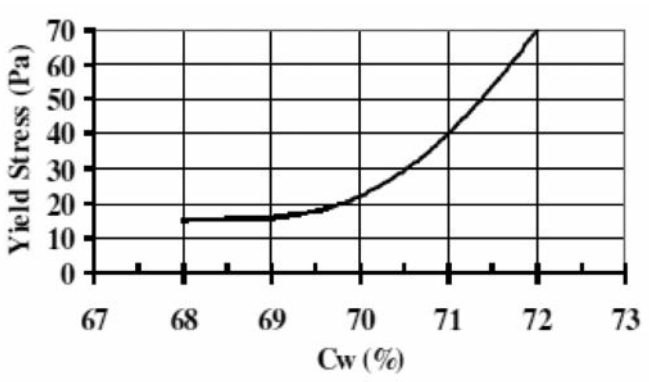


Figure 4. First guide indicator showing increasing yield stress with increasing concentration (Burgess, 2004)

Depending on the rheological behaviour of the slurry, discharge pipeline flows may need to be pumped in laminar or turbulent flow regimes. For example, for certain types of yield pseudoplastic applications where the slurry exhibits a shear thinning characteristic, rather than a laminar flow regime, it may be preferable to operate in the turbulent flow regime due to the possibility of solids settlement.

Considering the rheological properties exhibited by Bingham plastic slurries, turbulence effectively destroys the yield structure, causing the slurry to behave as a Newtonian fluid with viscosity roughly equal to the coefficient of rigidity.

Non-Newtonian pumping limitations for conventional centrifugal slurry pumps

Complex viscous and paste-like non-Newtonian slurries can negatively influence pumping performance. This has the potential to create unfavourable pumping conditions for conventional centrifugal slurry pumps.

The greater part of undesirable pump performance stems from design constraints, contributing to both a source of energy loss and an ineffectual slurry flow at the pump inlet and into the impeller eye. As yield-stress type slurries require a finite amount of shear to make them move, the viscosity of the slurry can trigger cavitation-related effects and result in a loss of pumping performance. This is evident in a conventional slurry pump at low flow rates. Additionally, the net positive suction head required (NPSHr) by a conventional slurry pump increases substantially when pumping viscous or paste-like non-Newtonian slurries. This can be attributed primarily to the variations of the slurry flow patterns into the impeller eye and through the vane passageways. As a conventional slurry pump impeller is inherently more efficient when handling Newtonian slurries, pumping viscous or paste-like non-Newtonian slurries entails certain trade-offs. Since wear relates to the progressive removal of the protective material from an elastomeric (rubber lining) or a metal (high-chrome iron) surface, the useful life of a conventional centrifugal slurry pump is reduced by erosive wear of the wetted components. Wear patterns are influenced by the size, shape, and hardness of particles in the slurry. However, as will be explained in the case study described later, encroaching on or operating in a two-phase viscous or paste-like mixture (which is not a true homogenous mixture) can have an exponential effect on abrasion and sliding wear in the pump. Although methods have been developed to reduce the effects of these viscous, paste-like slurries on the performance of conventional centrifugal pumps, success has been minimal until the introduction of the new AHF™ horizontal centrifugal froth pump technology.

Two separate field tests conducted on thickener underflow applications at mines in Zambia and Australia, successfully demonstrated that this new froth pump technology offered enhanced pumping performances of viscous and paste slurries.

The new Warman® AHF™ froth pump technology for concentrate thickening

Figure 5 shows the Dorr Olivier 60 ft phosphate concentrate thickener 11, the underflow from which was chosen to test the froth pump technology. Weir Minerals Africa was tasked to both evaluate the application and gather essential data in the lead-up to testing the new froth pump

technology on this viscous slurry application.

From the initial site visit, it was noted that this thickener (like the rest of the Foskor concentrate thickeners) was designed with a Y-piece underflow suction line.

Figure 6 shows the underflow cone section connected to the 200NB vertical suction column leading down to the Y-piece, complete with the installed pneumatically-operated isolation valves. This underflow piping system enabled the plant operators to redirect the slurry flow from the running pump to the standby pump or *vice versa*.

As depicted in Figure 7, B-Frame rubber lined conventional centrifugal slurry pumps were installed as the running and standby thickener underflow pumps. The Centriseal (semi-dry) gland design required gland service water to flush, cool, and lubricate the glands.

With the development of the new Warman® AHF™ froth pump technology, these old-generation conventional-type slurry pumps are now deemed the 'historic approach' to pumping viscous thickener underflow slurries.

Data collection

Before any froth pump selection could be compiled for the thickener 11 underflow application, it was vital to gather and review strategic information. This necessitated assessing the following key aspects:

- The process flow diagram for the whole plant to fully understand where thickener 11 is positioned within the circuit
- The metallurgical mass balance for thickener 11, with special attention to the underflow criteria
- The thickener underflow particle size distribution (PSD)
- The thickener underflow flow rate data
- The thickener underflow pulp density data
- Specific pump data and component wear patterns.

Review of the metallurgical mass balance for thickener 11

Figure 8 represents a generic filtration metallurgical mass balance for the chosen thickener as received from operational personnel. From this figure, the mass balance index, as highlighted in yellow, was used as the 'generic



Figure 5. 60-ft Dorr Oliver phosphate concentrate thickener

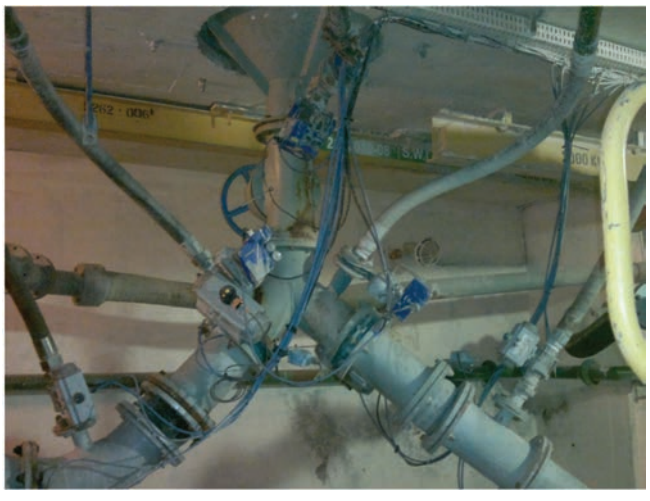


Figure 6. Thickener 11 underflow (pump suction side) piping configuration



Figure 7. B-Frame centrifugal (Centriseal) slurry pump

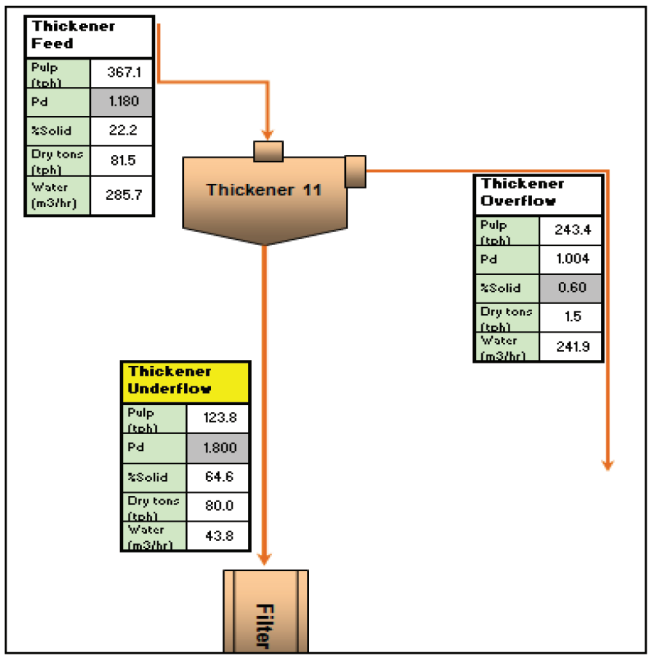


Figure 8. Representation of the metallurgical mass balance for thickener 11

mass balance' for the thickener 11 underflow application. At a thickened slurry density of 1800 kg/m³, it was noted that for a dry throughput of 80 t/h at a given dry density of 3200 kg/m³, the concentration by mass (C_m) and concentration by volume (C_v) would amount to 64.65% and 36.36% respectively. From this mass balance, the slurry flow rate was noted as 19.01 *l*/s.

Particle size distribution (PSD)

Table I shows the particle size distribution, as determined from an underflow sampling campaign. It should be noted that the above generic mass balance was based on a typical dry density of 3200kg/m³; however, from the sampling campaign it can be seen that the true dry density was 3170 kg/m³. These periodic fluctuations in the dry solids density are due to mining from two different open pits. This impacts the ore quality and metallurgical performance. Table I shows a distinct bimodal particle size distribution *i.e.* a coarse fraction that peaks between 200 to 300 μm and a fines fraction that appears to peak below about 50 μm.

Flow rate data

The flow rate for thickener 11 is measured by the flow meter in litres per minute, and recorded over a time scale of operational hours.

From more than 700 flow rate recordings, the average flow rate was noted to be 1374.63 *l*/min (22.91 *l*/s). This was slightly higher than the generic mass balance, and was most likely attributed to pumping at lower pulp densities. Flow rates occasionally peaked at 1688 *l*/min (28.13 *l*/s), with the highest recorded flow rate spiking at 2044 *l*/min (34.06 *l*/s). As the typical life expectancy for the conventional slurry pump wet end (elastomer impeller and liners) was around 3 to 5 months, poor pumping performance at the end of impeller/liner life accounted for the flow rates dropping down to below 950 l/min (15.8 l/s).

With the reconditioning of the pump, flow rates were restored to the abovementioned numbers. Even after fitting new impellers, it was noted that persisting erratic flow rate patterns were regularly observed. No satisfactory explanation could be given for this behaviour at the time of receiving the data, although there was some speculation that the positioning of the thickener rakes had an influence on variations of slurry feed into the underflow cone chamber.

Figure 9 shows typical supervisory control and data acquisition (SCADA) flow rate recordings of the conventional underflow slurry pumping system.

Table I
PSD of the underflow of thickener 11

PSD

Sieve size (µm)	Mass (g)	Weight (%)	Cum oversize (%)	Cum undersize (%)
+425	0.50	0.2	0.2	99.8
+300	8.20	3.6	3.8	96.2
+212	29.10	12.6	16.4	83.6
+150	37.00	16.1	32.5	67.5
+106	44.10	19.1	51.6	48.4
+75	44.00	19.1	70.7	29.3
+53	26.40	11.5	82.2	17.8
+38	8.40	3.6	85.8	14.2
-38	32.60	14.2	100.0	0.0
Total	230.30			

d50	110µm
SG (dry solids)	3.17 t/m³

Underflow slurry densities

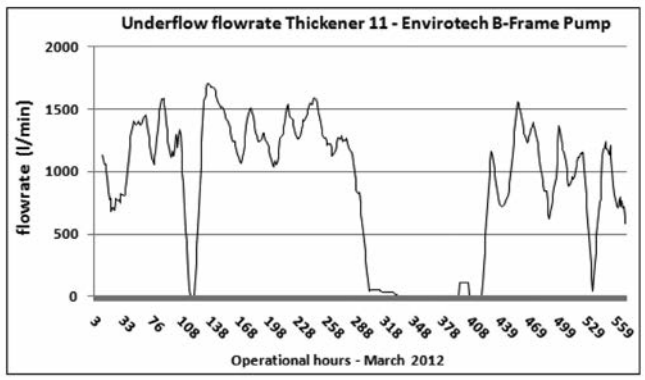
From more than 700 recordings, slurry densities were noted to range from around 1230 kg/m³ to very brief spikes of 1990 kg/m³. The average slurry density was 1776.32 kg/m³. This was lower than the generic mass balance, and was most likely attributed to the inability of a conventional slurry pump to handle slurries at high viscosity thresholds. Short impeller life also contributed to the underflow pumping being negatively influenced by the gradual decline in slurry densities.

At this point it is important to note that the measurement and feedback readings from the underflow densitometer and flow meter are used to control the speed of the thickener underflow pumping unit. The primary function of the thickener underflow pump is therefore to control the thickener, and the delivering of the underflow slurry to the belt filter is the secondary function (Vietti, 2014).

Pump data and pump component wear patterns

The data discussed above indicated that the thickener 11 underflow pump application was very complex and challenging.

With limited historic rheology information at hand, it was concluded that the selection of the conventional centrifugal slurry pump was based on phosphate slurry thickening experience. In order to establish where the conventional slurry pump was operating on the plant system curve, the basic hydraulic principles relating to the generation of the plant system curve were adopted. This involved measuring the load current drawn by the motor, measuring the true motor speed and pump speed using a stroboscope,



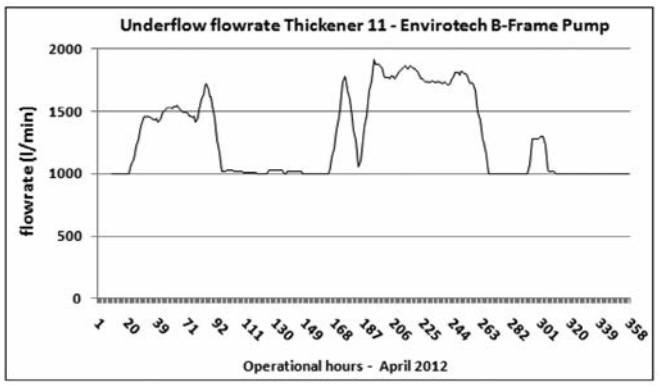


Figure 9. SCADA flow rate recordings for thickener 11

calculating the differential head derived from the difference between the static suction and static discharge heights, and reviewing the suction/discharge piping arrangement.

The discharge piping arrangement was a 125NB steel rubber-lined (116 mm ID) pipe, 92 m long, with 10 × 90°, 4 × 45° bends and a static differential head of 18.2 m. No shear stresses were included in any calculations, but a dynamic friction head loss of 6.90 m of fluid per 100 m of pipe was assumed.

From this information a rudimentary multi-system curve analysis was generated (Figure 10).

Figure 10 depicts a multi-system curve scenario that extends over the typical high and low flow rate and density fluctuations. The deviation between the red block (duty point for water) to the blue block (primary duty point for slurry) relates to the pump head deration.

The top end of the curve simulation reflects the primary duty point of 27 *l*/s at 1690 kg/m^3 for 31.34 m (derated) total static dynamic head (TSDH) at 1157 r/min pump speed.

The bottom end reflects the secondary duty point of 16 *l*/s at 1990 kg/m^3 for 20.78 m (derated) TSDH at 958 r/min pump speed. In between the top and bottom zones, the superimposed dots represent the vast range of possible duty points. In most instances, these duty modulations were the result of the controlling philosophy based around the flow meter and densitometer recordings, transmitted through the SCADA to the variable speed drive (VSD). Based on the received information, the VSD would either speed up or slow the pump down.

Although the above represents estimations of the typical duties, it is clear that the conventional slurry pump was operating in unfavourable duty zones, situated below the 35% position from the best efficiency point (BEP).

For this type of conventional slurry pump design, high localized wear will be significantly amplified when the pump is allowed to operate at these far left BEP duties.

Non-Newtonian slurries undergo a certain amount of shearing inside the impeller and pump casing, but the amount of shearing is dependent on the size of the pump, the velocities and flow rate through the pump.

Considering conventional slurry pump performance, the NPSHr while pumping viscous non-Newtonian slurries increases substantially compared with pumping Newtonian slurries. The change in viscosity can trigger cavitation-type effects, which are more pronounced for conventional slurry pump impeller designs. At flow rates ≤ 50% of BEP, internal vortex pockets can form within the pump, and these represent sources of energy loss. The cavitation-type behaviour has a destructive effect around the underside area near to the leading edges of the impeller vanes, where a sudden drop in fluid pressure is most likely to occur. This cavitation damage is not always detectable as it is often masked by particle erosion, which occurs simultaneously due to solid particles in the slurry. The conventional closed vane (double shrouded) slurry pump impeller design produces very low levels of shear and kinetic energy needed to move the slurry through the inlet pipe and into the pump impeller eye, thus some part of recirculation within the pump contributes to further wear. This is attributed mainly to the variations of the viscous or non-Newtonian slurry flow patterns into the impeller eye and through the vane passageways. The severity of the erosion and gouging depends on the ratio between the operating flow rate and the best-efficiency flow rate. Under low flow rate conditions, recirculation can contribute to secondary gouging damage. Secondary gouging eddies are susceptible to forming in a number of locations, but form mostly

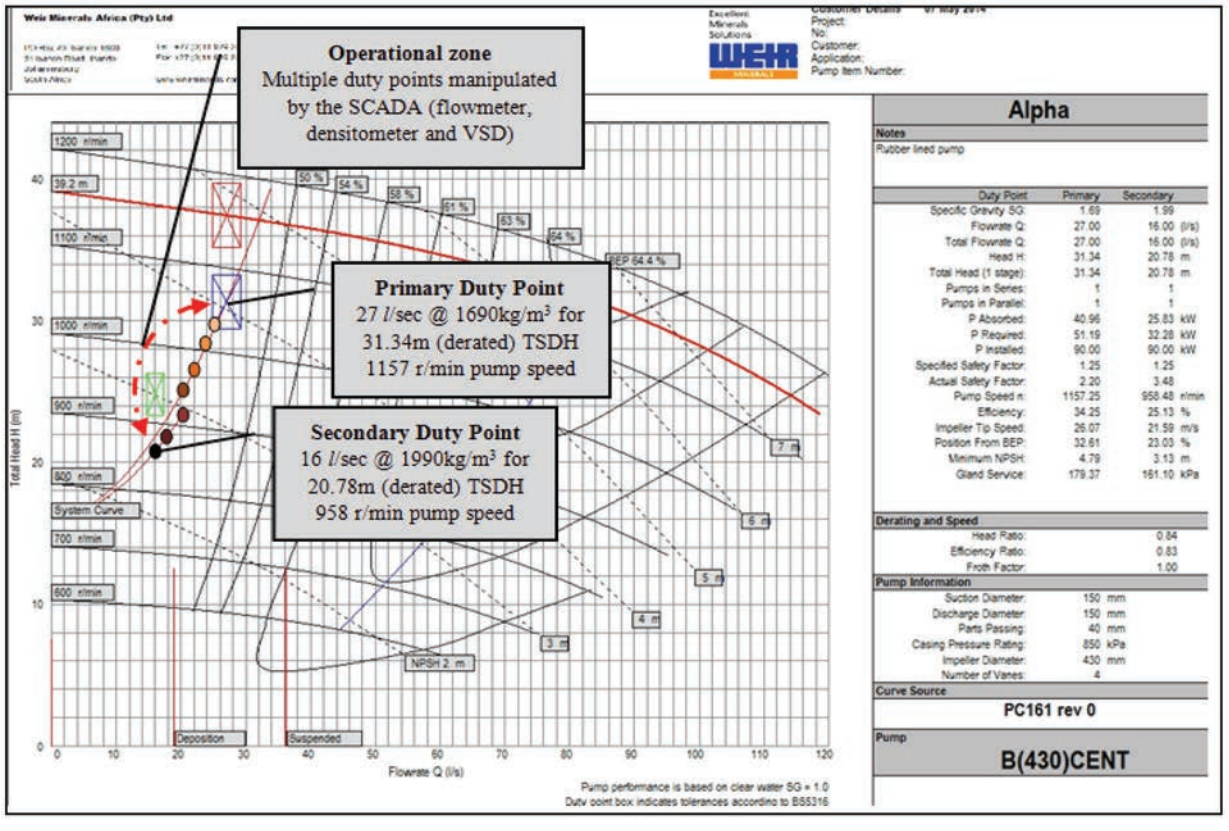


Figure 10. Multi-system curve scenario for the conventional B-Frame slurry pump

around the vane discharge tips, impeller shrouds, and corresponding liner areas.

The clearances between the impeller shrouds and the suction/drive side liners are rapidly altered by the high localized wear rates. Thereafter secondary and more insistent gouging eddies may be formed within these eroded zones. These secondary eddies tend to aggressively erode away at, or around, a worn cavity within the protective lining, significantly increasing the severity of the localized wear. This continues until the wear reaches the steel boundary layer (as shown in Figure 11 by the yellow arrow indicating secondary eddy damage on the back impeller shroud of the conventional slurry pump). With no protection lining, the secondary eddies rapidly erode the exposed steel area, progressively destroying the impeller. With increased recirculation and declining efficiency, the pump would eventually begin to self-destruct. In extreme cases, the unfavourable pumping conditions were sufficiently severe to crack open the 850 kPa pressure-rated casings.

The root cause investigations into the casing failures were inconclusive, although fluid hammering resulting from rapid flow rate changes or sudden flow stoppages (as typically seen in Figure 9A) could have caused pressure surges being transmitted back to the pump.

Figures 11–14 show failure patterns and wear of the conventional slurry pump components and bear testimony to the above discussions.

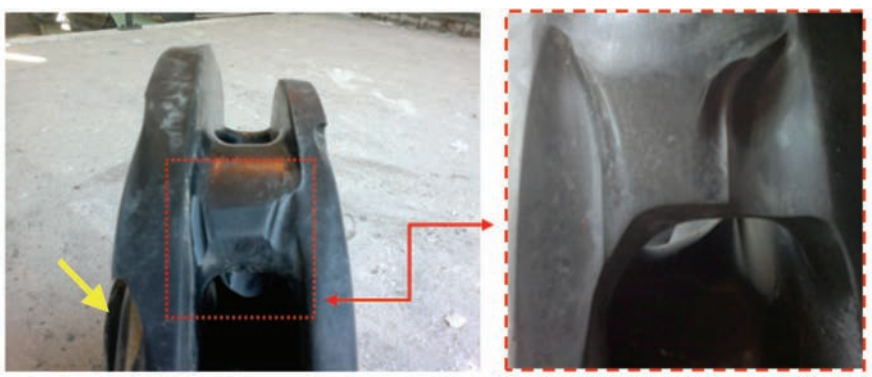


Figure 11. Wear damage to the back shroud and discharge sections of the centriseal impeller vanes

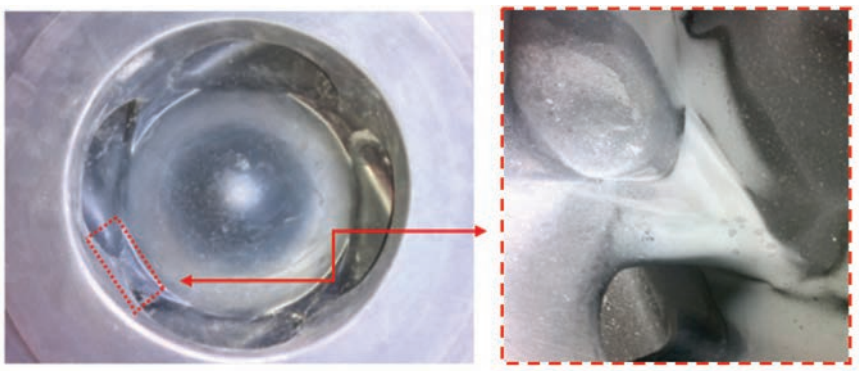


Figure 12. Wear damage to leading sections of the impeller vanes

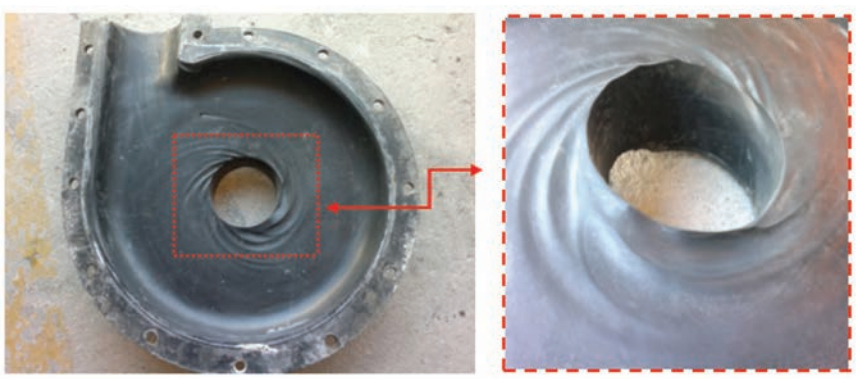


Figure 13. Spiral wear damage to the back liner



Figure 14. Multiple suction casing failures

Comparing the past approach to the new preferred approach

Figures 15 and 16 show the cross-sectional views of the conventional horizontal centrifugal slurry pump compared with the new horizontal centrifugal froth pump technology.

The sectional view of the conventional slurry pump indicates the closed vane (double shrouded) slurry pump impeller. The generic suction inlet and impeller design produces very low levels of shear and kinetic energy that are needed to efficiently move viscous slurry through the inlet and into the pump impeller eye.

The sectional view of the new froth pump technology clearly shows the large open vane flow inducer froth pump impeller, with its greatly enlarged cover plate pump inlet and matching throat bush liner. This design offers vast technological improvements in pumping viscous and paste-like non-Newtonian slurries.

Figures 17 and 18 compare the inlet designs of the conventional slurry pump and the new froth pump, contextualizing the suction inlet discussion.

It is important to note that compared to the 850 kPa rated casing pressure of the Envirotech® Centriseal slurry pump, the Warman® froth pump has a 1400 kPa casing pressure rating, nearly double than that of the Centriseal pump.

The innovative design of new the froth pump inlet is superior to the inlet design of conventional centrifugal slurry pump. This patented inlet design has the effect of reducing the NPSHr, increasing the flow rate, and improving viscous slurry pumping efficiency, compared to a conventional slurry pump for the same duty.

Noticeably from Figure 19, the unique froth pump impeller has open inducer vanes that protrude into the large intake throat area. This design extends the vane leading edges and serves to draw viscous and paste-like slurries into the eye of the impeller, reducing the potential for plugging or sticky slump flow issues (Burgess, 2004).

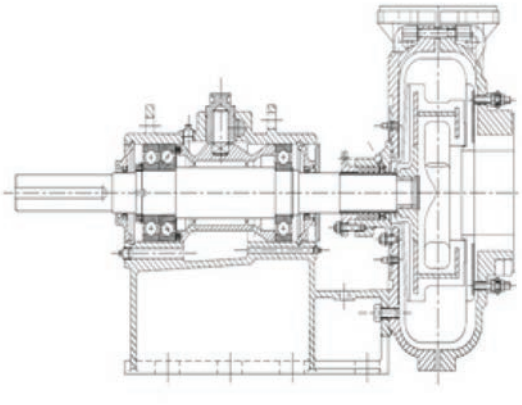


Figure 15. Centriseal slurry pump

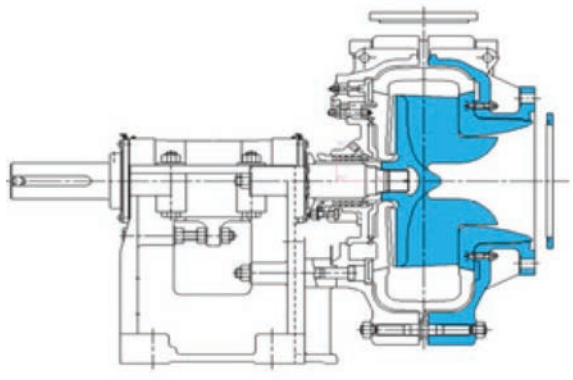


Figure 16. Warman® AHF™ froth pump



Figure 17. Conventional slurry pump inlet



Figure 18. New froth pump inlet



Figure 19. Slurry-inducing and shear-thinning vane design of the froth pump



Figure 20. Conventional slurry impeller



Figure 21. New froth pump impeller

Duty Point	Primary	Secondary	
Specific Gravity SG:	1.99	1.70	
Flowrate Q:	23.50	21.83	(l/s)
Total Flowrate Q:	23.50	21.83	(l/s)
Head H:	22.65	23.77	m
Total Head (1 stage):	22.65	23.77	m
Pump Speed n:	1622.59	1621.91	r/min
Efficiency:	37.13	37.20	%
Impeller Tip Speed:	21.84	21.83	m/s
Position From BEP:	52.16	48.47	%
Minimum NPSH:	2.48	2.34	m
Gland Service:	542.16	496.49	kPa

Figure 22. Primary and secondary 'first guide approach' duty predictions

Consequently, the impeller vanes are able to induce a swirl effect in the viscous slurry around the immediate intake pipe/throat bush area. This promotes significant shear-thinning properties while improving kinetic energy, and affording the sheared, viscous slurry smooth entry into the impeller eye and passageways.

Figures 20 and 21 contrast the conventional 'historic approach' impeller design to the new froth pump impeller design for pumping viscous and paste like non-Newtonian (and frothy) slurries.

The Warman® AHF™ froth pump testing campaign on Thickener 11

From the anticipated duties reflected in Figures 22 and 23, the 3CC-AHF™ froth pump was selected (based on an approximated 'first guide approach').

Primary (design) duty: 121 t/h at a C_m of 72.36%, RD = 1.99, and a C_v of 45%

Secondary (operational) duty: 80 t/h at a C_m of 58.98%, RD = 1.70, and a C_v of 31.28%

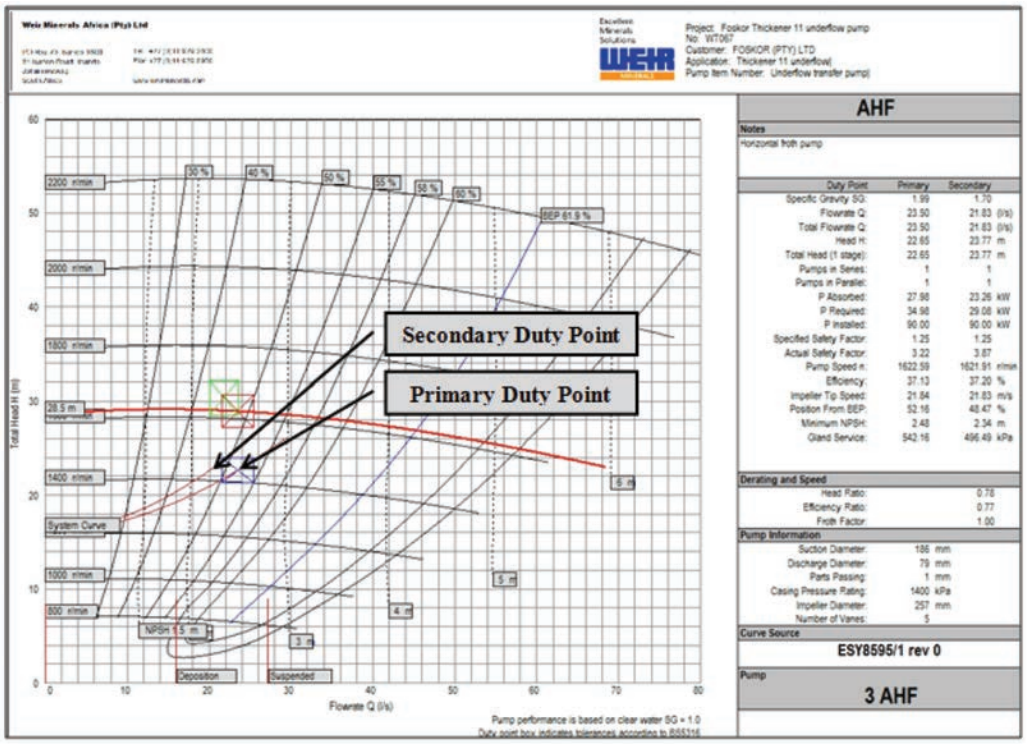


Figure 23. Primary and secondary system curve predictions for the 3CC-AHF™ froth pump

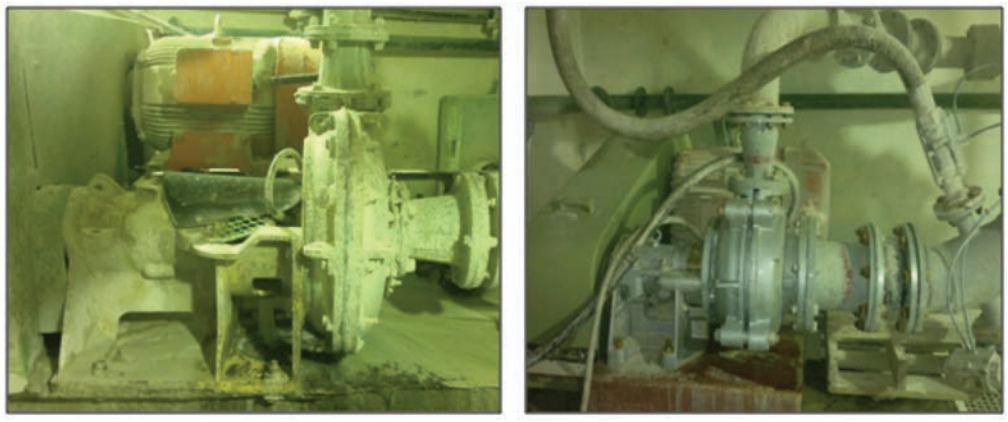


Figure 24. Before and after retro-fitment

The required pump speed for both duties coincided at 1622 r/min.

Installation and phase 1 of the test work

Early in 2013, the conventional centrifugal slurry pump was removed from service and the new Warman® 3CC-AHF™ froth test pump was installed in its place. Figure 24 shows the equipment before and after installation, with the minor suction pipeline modifications carried out to suit the 3CC-AHF™ froth pump suction flange details.

Due to the high static suction head that exceeded the capabilities of the 3CC-AHF™ dry gland expeller head, the froth pump was configured as a wet gland expeller-less stuffing box arrangement for a gland service flow rate of 0.9 *l*/s. The installed 90 kW 4P 525 V electric motor was re-used.

After commissioning, it was noted that the 3CC-AHF™ froth test pump running at 1622 r/min did not have sufficient hydraulic energy to induce a sustainable flow rate at the open end of the discharge pipe section. This was due to a lack of rheological data and incorrect system curve predictions.

Phase 2 of the test work

It was important to understand if the difficulty in achieving a suitable discharge flow rate was related to a complex rheology issue, or a misinterpretation of the TSDH (or a combination of both).

As the 3CC-AHF™ froth test pump complete with a 257 mm diameter impeller was considered as the preferred choice between the smaller 2-AHF™ and the larger 4-AHF™ froth pump, it was decided to commence with pump speed experimentation, progressively increasing the pump speed through pulley ratio changes until the desired discharge flow rate was achieved. Based on available standard pulley size ranges, and ensuring that the final pump speed did not exceed the critical design limitations of the 3CC-AHF™ froth pump, the new speed selections were

identified as 1868 r/min, 2054 r/min, and 2110 r/min.

On completing the pulley ratio change to achieve a new pump speed of 1868 r/min, the pump was started up again. The new speed range demonstrated a very slight flow improvement with a spluttering-type flow rate effect seen at the open discharge pipe end.

This was obviously still well below the maximum and desired operation duty. The next 2054 r/min pulley ratio was installed on the 3CC-AHF™ froth pump.

Phase 3 of the test work

Following this speed adjustment, the pump immediately demonstrated a greatly improved flow rate performance. However, at the desired flow rate conditions, the pump head and power input were higher than originally anticipated. This condition was more pronounced at discharge slurry densities around 1800 kg/m^3, with optimum results seen at densities ≥1900 kg/m^3. The SCADA system recorded a slurry density of 1906 kg/m^3 and a 1478 *l*/min (24.63 *l*/s) flow rate as transferred by the thickener 11 underflow froth test pump.

It became evident from this test work that the significant increase in friction head and absorbed power related to the complex rheology behavioural changes that took place within the froth pump impeller and the discharge piping system.

Due to the unique froth pump impeller design, it was expected that the flow patterns near the impeller inlet would be positively affected by the shearing. However, the expectation was to achieve this at a pump speed well below the required 2054 r/min speed amendment. The absorbed motor power calculation indicated that at this duty point, the absorbed power had increased to 70% of the kW installed. In the absence of any rheology data, the following findings proved valuable. Increasing the froth pump speed to over 2000 r/min:

- Substantially increased the shear rate
- Increased the slurry velocity
- Changed the slurry viscosity.

Although the Phase 3 Warman® 3CC-AHF™ froth pump demonstrated significantly improved pumping performance compared to the conventional centrifugal slurry pump, it was predicted that at 2054 r/min, the 27.4 m/s impeller tip speed would contribute to accelerated impeller wear rates.

Phase 4 of the test work

As a result of the accelerated wear rate predictions, the 3CC-AHF™ froth pump was replaced with the larger 4E-AHF™ froth pump. The focus was now to be directed towards understanding the effect of using the next larger size froth pump with a 388 mm diameter impeller.

As both the maximum and operational duty points would be positioned very far to the left of BEP, it was further decided that before any plant system curves were simulated, a representative slurry sample would be extracted from the thickener 11 underflow sampling point and sent to the Minerals Processing Division of Mintek in Randburg, South Africa.

A 25 kg slurry sample was extracted from the thickener underflow stream, and an 8 kg subsample sent for rheology testing. Figure 25 shows the dried packaged slurry samples awaiting the rheology testing process, and Table II shows the particle size distribution of the sample as received.

Figure 26 shows the particle size distribution data (as dry screened product received from Foskor). The thickener underflow ore sample had a d_{90} of 250.10 μm and a d_{50} of 116.00 μm.

The objective of this complex rheology study was to characterize the behaviour of the thickener underflow slurry at five different slurry relative densities of 1.7, 1.8, 1.9, 2.0, and 2.1. The slurries were characterized by calculating the rheology properties, with specific focus on viscosity and yield stress. The dry density of the ore was determined using a Micromertics AccuPyc ll 1340 Gas Pycnometer, and was found to be 3142.25 kg/m^3.



Figure 25. Packaged samples

Table II
PSD screening results

Size Fraction Micron	Mass % Passing	Cumulative Mass % Passing
512.5	0.50	100.00
362.5	8.23	99.50
256.0	16.09	91.27
181.0	19.22	75.18
128.0	18.64	55.96
90.5	11.84	37.32
64.0	10.16	25.48
45.5	7.76	15.32
19.0	7.57	7.57

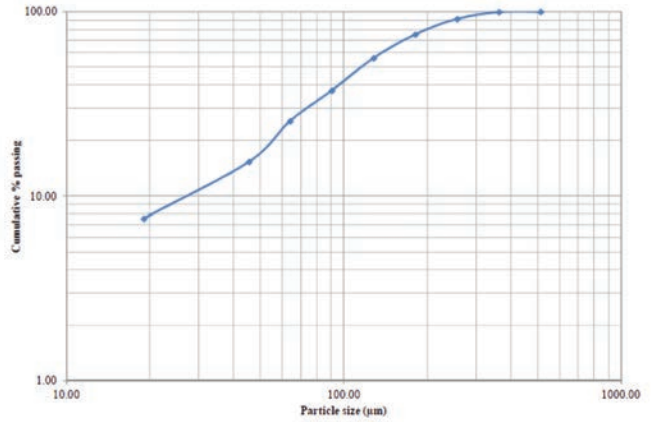


Figure 26. Thickener underflow particle size distribution

Table III
Concentration matrix used to prepare the slurry test samples

ρs (kg/m^3)	ρl (kg/m^3)	*x* (wt%)	ρsl (kg/m^3)	Slurry SG
3142.25	1000.00	60.00	1692.20	1.69
		65.00	1795.79	1.80
		70.00	1912.89	1.91
		73.00	1990.77	1.99
		76.00	2075.27	2.08

(ρs) = density of solids (kg/m^3)
(ρl) = density of water (kg/m^3)
(ρsl) = density of slurry (kg/m^3)
(*x*) = solids concentration (wt%)

The slurry was repulped to conduct five slurry tests at the following densities: 1692.20 kg/m^3, 1795.79 kg/m^3, 1912.89 kg/m^3, 1990.77 kg/m^3, and 2075.27 kg/m^3.

Table III, compiled by Mintek, represents the concentration by weights of the mixed slurry densities, as repulped from the 3142.25 kg/m^3 dry solids (Foskor ore).

The rheology testing was conducted using a Physica Rheolab QC rheometer fitted with a vane-type bob and cup configuration as shown in Figure 27.

All rheology tests were conducted under laboratory conditions and at room temperature.

A shear rate range between 1 s^{-1} and 800 s^{-1} was used by first pre-shearing the slurry at a constant 800 s^{-1} to prevent any settling of the solids. A downward slope was then generated to measure the shear stress from 800 s^{-1} to 1 s^{-1}.

Shear stress and apparent viscosity (viscosity at a value of shear rate) were recorded based on the set shear rate range. Shear stress versus shear rate data obtained was fitted with a model exhibiting behaviour of the slurry to determine the viscosity and yield stress.

Plots of rheograms (shear stress versus shear rate flow curves) were generated.

Shear rates from 250 s^{-1} to 600 s^{-1} were used to analyse the data for the slurries at densities of 1700 kg/m^3 and 1800 kg/m^3. This was necessary as the values less than 250 s^{-1} did not generate data that could be interpreted to fit with a model. A shear rate range from 1 s^{-1} to 600 s^{-1} was used to analyse the data for the slurries at densities of 1900 kg/m^3,



Figure 27. Physica Rheolab QC rheometer with a vane geometry

2000 kg/m^3, and 2100 kg/m^3. This shear rate range was selected as the results could easily be interpreted.

The slurries at densities of 1700kg/m^3 and 1800 kg/m^3 were found to exhibit yield dilatant (shear thickening behaviour). This behaviour was further confirmed by an increase in apparent viscosity with increasing shear rate, as seen in Figure 28.

Table IV shows the apparent viscosity and yield stress values for the slurry densities of 1700 kg/m^3 and 1800 kg/m^3. The apparent viscosity was determined at two values of shear rate *i.e.* 300 s^{-1} and 500 s^{-1}.

However, for the slurry densities of 1900 kg/m^3, 2000 kg/m^3, and 2100kg/m^3, the shear rate range from 1 s^{-1} to 600 s^{-1} could be used to analyse the data as this range could be interpreted.

The pseudoplastic model was used to fit the data for these slurry densities, and as seen in Figure 29, these slurries were found to be shear-thinning, exhibiting a yield pseudoplastic behaviour.

Table V shows the yield stress and viscosity values that were obtained from the yield pseudoplastic model fits.

Figure 30 shows the complex rheogram plots of shear stress against shear rate for all the slurries tested. The slurries at slurry densities of 1700 kg/m^3 and 1800 kg/m^3 exhibit yield dilatant shear thickening (behaviour associated

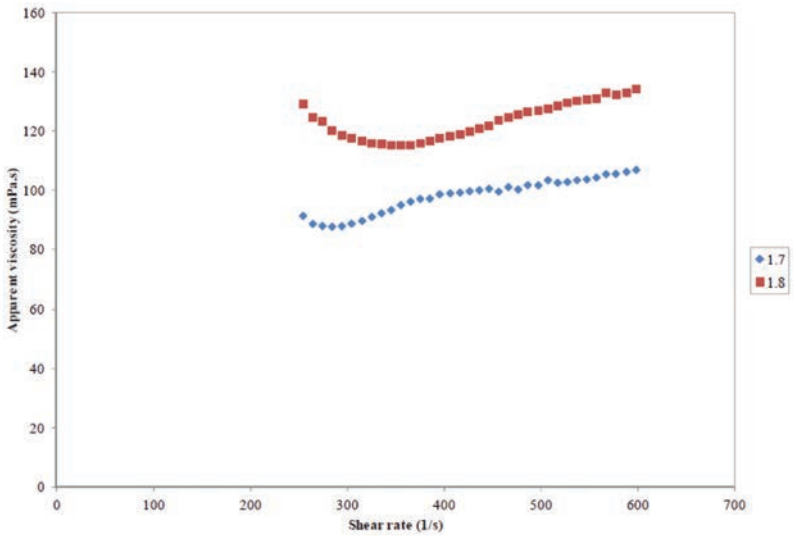


Figure 28. Shear thickening behaviour, 1700 kg/m^3 and 1800 kg/m^3 samples

Table IV
Yield stress and viscosity values for the yield dilatant slurries at densities of 1700 and 1800 kg/m³

Slurry SG	HB Yield stress (Pa)	n	K	Apparent viscosity (mPa.s)	
				at 300 (s^{-1})	at 500 (s^{-1})
1.7	7.50	1.56	2.70E-03	65.61	87.30
1.8	18.05	1.81	5.72E-04	58.83	89.08

with a yield stress). For the slurry densities of 1900 kg/m³, 2000kg/m³, and 2100 kg/m³, it is worthwhile noting that these slurries seem to initially exhibit a yield pseudoplastic behaviour followed by a slight dilatant behaviour at approximately 350 s^{-1}. However, this stems from the method adopted in the rheology tests. The behaviour above 350 s^{-1} remained one of yield pseudoplastic shear thinning (as seen in Figure 29).

Figure 31 shows the plot of yield stress against the different slurry densities tested. It should be noted that for the slurries with densities of 1700 kg/m³ and 1800 kg/m³, the yield dilatant stress was extrapolated from the data.

The Bingham yield shear stress was also extrapolated for the slurries with densities of 1900 kg/m³, 2000 kg/m³, and 2100 kg/m³. This plot confirmed the increase in yield shear stress with the increase in slurry density (since two different models were used).

An exponential relationship between the yield shear stress and slurry density can be observed.

There is a significant jump in the Bingham yield shear stress from 2000 kg/m³ (52.23 Pa) to 2100 kg/m³ (93.14 Pa), which may indicate that the slurry density of 2000 kg/m³ is the critical slurry density for pumping.

Table V
Yield stress and viscosity values for the yield pseudoplastic slurry densities of 1900, 2000, and 2100 kg/m³

Slurry SG	Yield stress (Pa)		Bingham viscosity	
	True	Bingham	(Pa.s)	(mPa.s)
1.90	19.30	40.83	0.10	100.28
2.00	23.50	52.23	0.15	152.06
2.10	52.22	93.14	0.25	245.89

Figure 32 illustrates the effect of slurry density on the Bingham plastic viscosity. The apparent viscosities for the slurries at densities of 1700 kg/m³ and 1800 kg/m³ were not plotted as at this point the optimum shear rate existing in the pump at a particular speed had yet to be established.

The values obtained from the yield pseudoplastic model bestowed greater confidence.

A significant jump in Bingham plastic viscosity was also observed from 2000 kg/m³ (152.06 mPa.s) to 2010 kg/m³ (245.89 mPa.s), which may indicate that 2000 kg/m³ is the critical slurry density for pumping.

An exponential relationship exists between the Bingham viscosity and slurry density.

Phase 5 of the test work

From the vital knowledge gained through the initial 3CC-AHF™ froth pump test campaign as well as the rheology test results from Mintek, it became apparent that as slurry densities increase from 1700 kg/m³ to 2100 kg/m³, there would be an exponential increase in yield stress required to get the slurry to flow (as per Figure 31).

The Mintek results further confirmed that shear rates for the denser slurries followed a shear-thinning in yield pseudoplastic behaviour, whereas the lower density slurries followed shear-thickening in yield dilatant behaviour. This indicates that higher friction heads should be expected when pumping the 1700 kg/m³ to 1800 kg/m³ slurries.

As the 4E-AHF™ froth pump has an impeller 50% larger than the 3CC-AHF™ pump impeller, it was expected that the larger inducer vane impeller would be more effective at pumping the higher density yield pseudoplastic slurries (≥1800kg/m³ to 2100 kg/m³).

In conjunction with the rheology data from Mintek, a primary duty site system curve review revealed that a

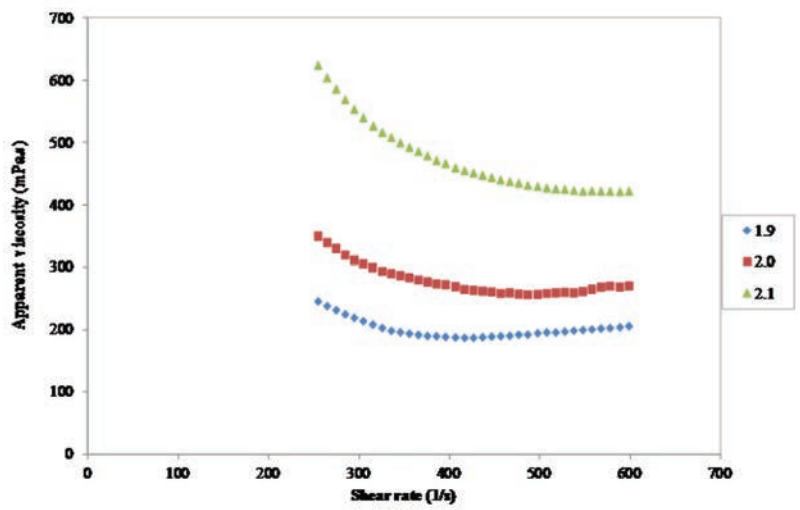


Figure 29. Shear-thinning behaviour, 1900 to 2100 kg/m³ samples

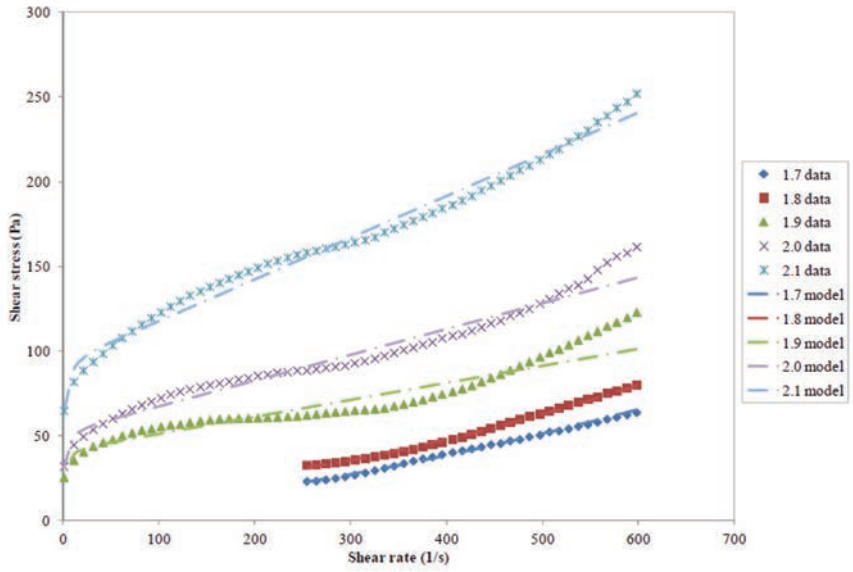


Figure 30. Shear stress vs. shear rate flow curves for all the slurries tested

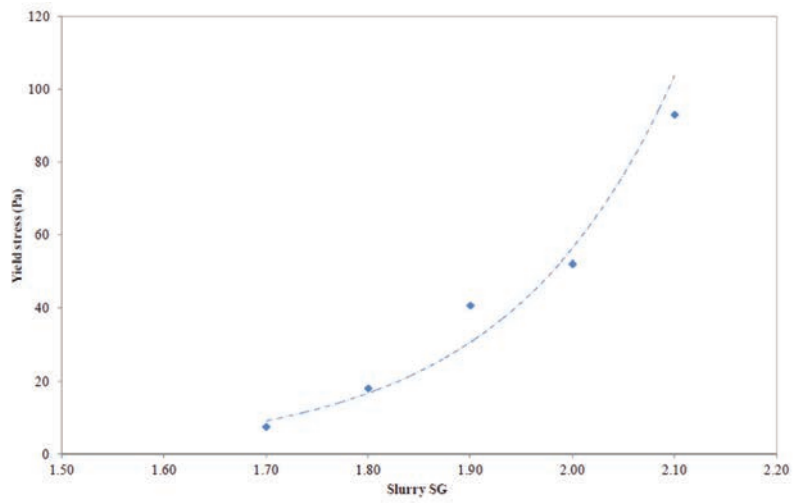


Figure 31. Effect of slurry SG on the yield stress

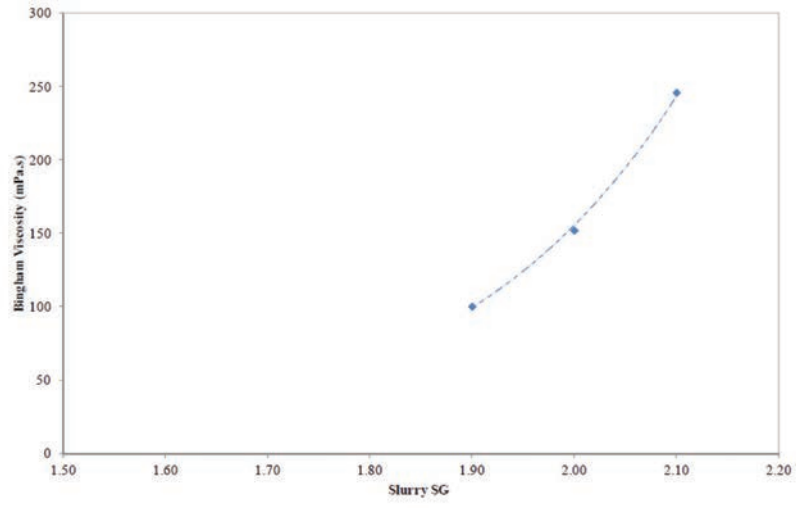


Figure 32. Effect of slurry density on viscosity

TSDH of 21.26 m for a 20.00 *l*/s flow rate at a slurry density of 2000 kg/m³ was to be expected. From the Bingham viscosity in Table V, the calculated Reynolds number for this duty was above 2000 but lower than 4000 (seen as a transitional flow regime). It was estimated that 28% of the 21.26 m head would be attributed to site system losses.

However, the secondary duty site system curve review revealed a TSDH of 28.45 m for a 24.75 *l*/s flow rate at a slurry density of 1800 kg/m³.

From the 300 s-1 and 500 s-1 apparent viscosities in Table IV the calculated Reynolds number for this duty was well above 4000, indicating a turbulent flow regime. It was estimated that 45% of the 28.45 m head was attributed to site system losses.

The anticipated duties are reflected in Figure 33.

From the system calculations, it was found that for operational duty, the 4E-AHF™ froth pump had to be designed to run at 1064 r/min for a 94% VSD set-point.

A drive pulley selection based on using a SPB 180 mm 5-groove motor pulley and a SPB 250 mm 5-groove pulley provided an ideal final drive speed of 1062 r/min.

Anticipating flow rate and slurry density fluctuations, the installed VSD would be used to control the pump speed within an acceptable predetermined range of 1130 r/min (as the high speed duty – 100% VSD set-point), and 990 r/min (as the low speed duty – 85% VSD set-point).

Installation and commissioning of the new Warman® 4E-AHF™ froth pump

After the removal of the initial 3CC-AHF™ froth pump, minor modifications were needed to the base plate and the suction line so as to accommodate the larger 4E-AHF™ froth pump. In contrast to the 3CC-AHF™ froth pump, the larger 4E-AHF™ froth pump with the Hi Seal® expeller design was capable of generating sufficient expeller head to overcome the high static suction head conditions.

Figure 34 shows the suction line before and after modifications required to replace the 3CC-AHF™ froth pump with the larger 4E-AHF™ froth pump.

After starting up the 4E-AHF™ froth pump, the grease-lubricated Hi Seal® expeller design demonstrated superb dry gland sealing performance.

Under the complete control of the VSD, the speed

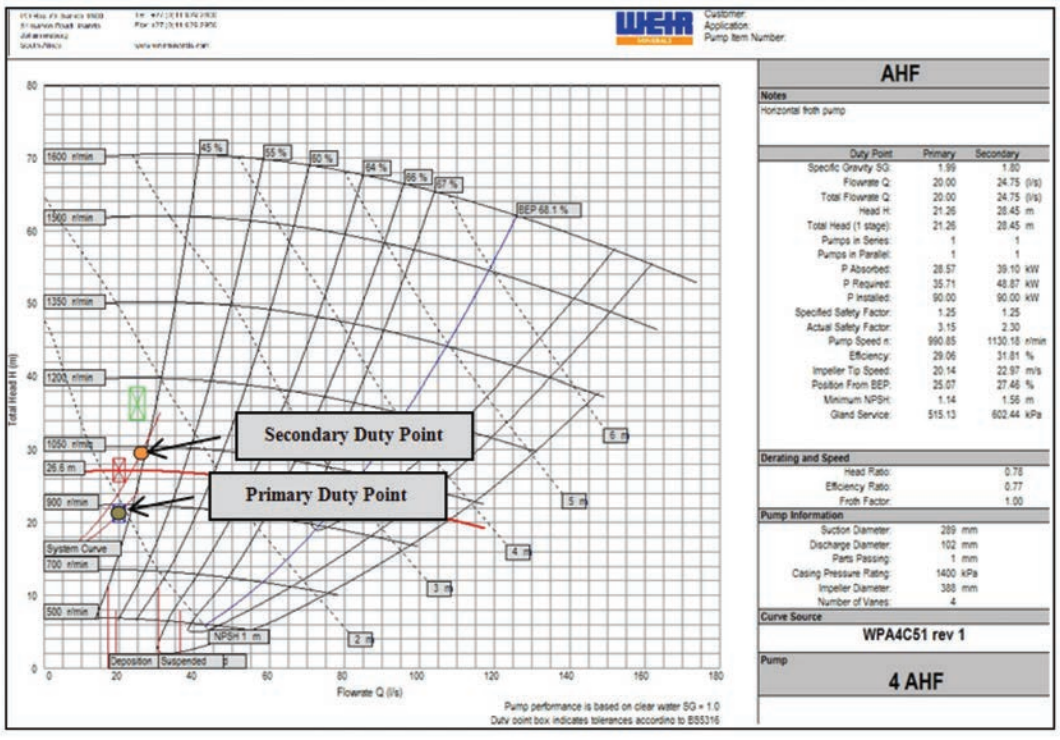


Figure 33. Primary and secondary system curve predictions for the 4E-AHF™ froth pump



Figure 34. Before and after retrofitment process



Figure 35. The 4E-AHF with the Hi Seal® expeller in full operation

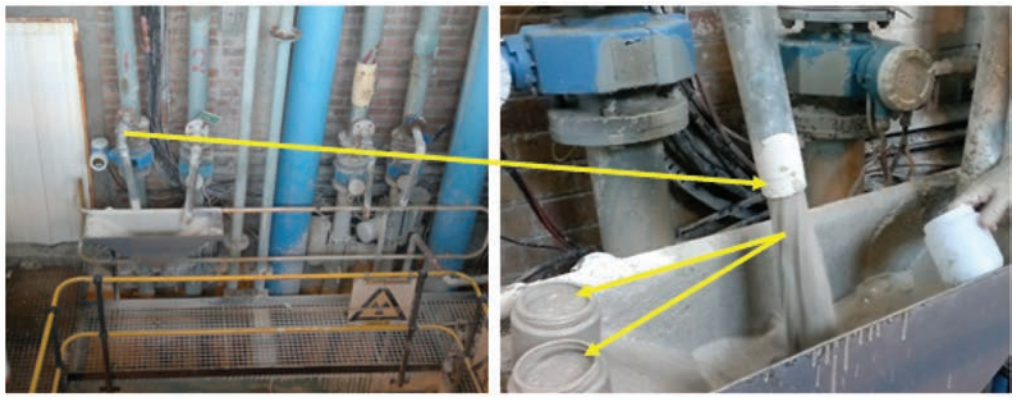


Figure 36. The sampling station and sampling in progress

fluctuations made no difference to the performance of the Hi Seal® expeller. Apart from a slight trickle of dirty water leaking from the gland at abnormally low pump speeds (800 r/min), the gland area remained completely dry.

Figure 35 depicts the dry gland sealing of the 4E-AHF™ froth pump under full pumping operation.

From the start-up of the larger 4E-AHF™ froth pump, the pumping performance improved noticeably compared with the previous 3CC-AHF™ froth pump tests.

Despite the froth pump operating far over to the left hand side of BEP, there was no influence on the pumping performance. No unfavourable signs of cavitation, such as vibrations, rumbling, excessive flow rate fluctuations, or elevated bearing temperatures were detected.

The elimination of cavitation was attributed to efficient inducer vane performance and improved NPSHr characteristics, whereby the absolute pressure at the froth pump impeller eye exceeded the vapour pressure by a suitable margin. This was further confirmed by the SCADA recordings, which demonstrated more constant flow rates with steadier slurry densities being seen above 1960 kg/m^3.

Although the SCADA data recordings were extremely useful, it was noted that density readings never exceeded the 2000 kg/m^3 parameter. This was either a result of very accurate thickener underflow control, or it related to some sort of capped densitometer reading. To further investigate this phenomenon, it was decided to carry out sampling campaigns of the underflow slurry pumped by the 4E-AHF™ froth pump. The sampling point was situated on the vertical discharge pipe column, directly above the installed densitometer and the flow meter.

Nearly 50 samples were taken over a six-week period, all of which were then sent to the Foskor laboratory for analysis. Figure 36 shows the sampling station and the capturing of the dense underflow slurry in sampling pots.

Although some of the analysed samples did indicate slurry densities below 1800 kg/m^3, most of the samples revealed the densities to be above 1950 kg/m^3. On many occasions the densities transferred by the 4E-AHF™ froth pump exceeded the capped 2000 kg/m^3 SCADA readings. Sampling results confirmed that the pumped slurry densities could easily peak at 2126 kg/m^3.

Table VI shows some of the extracted sampling results.

It was later discovered that the densitometer had been calibrated to record slurry densities ≤2000 kg/m^3. The SCADA would consequently also have been set to 2000 kg/m^3, since it's range needed to be identical to that of the densitometer.

It was assumed that as the previous conventional slurry pump was incapable of sustaining underflow pumping at these high slurry densities, calibrating to 2000 kg/m^3 had been practical.

Figure 37 is a typical snapshot of the SCADA recording the performance of the 4E-AHF™ froth pump over a period of about 52 hours. The density and flow rate recordings were measured in units of kg/m^3 and *l*/min, and represent a more stable trend than was seen with the conventional slurry pump (Figure 9).

As the SCADA recordings ended at a slurry density of 2000 kg/m^3, the round blue dots represent what would have been expected as the typical density curve trend, with the broken blue line indicating the highest sampled peak value (all based on sampling test results).

From the site system curve calculation, it was seen that

Table VI
Results from some of the slurry sampling campaigns

Reference				T11	T11	T11	T11	T11	T11	T11	T11
Reference				10	15	21	25	33	39	42	44
Note				AHF Pump	AHF Pump	AHF Pump	AHF Pump	AHF Pump	AHF Pump	AHF PUMP	AHF PUMP
Mass Pulp	=	Mp	kg	1.2956	1.1018	1.0387	1.0733	1.0823	1.0421	1.0005	1.0933
Mass Solids (Dry)	=	Ms	kg	1.0132	0.8051	0.7771	0.8045	0.8225	0.7805	0.7204	0.7928
Mass Water = Mw	=	Mp-Ms	kg	0.2825	0.2967	0.2615	0.2688	0.2598	0.2616	0.2802	0.3004
SG SOLIDS	=	SGs	kg/l	3.1000	3.1000	3.1000	3.1000	3.1000	3.1000	3.1000	3.1000
Container or Pulp Volume	=	v	liter	0.5300	0.5300	0.5300	0.5300	0.5300	0.5300	0.5300	0.5300
Then Dry method	Pulp Desity =		kg/l	2.126	1.980	2.028	2.032	2.061	2.030	1.952	1.966
And Wet method Pulp	Density =	m/v =	kg/l	2.445	2.079	1.960	2.025	2.042	1.966	1.888	2.063

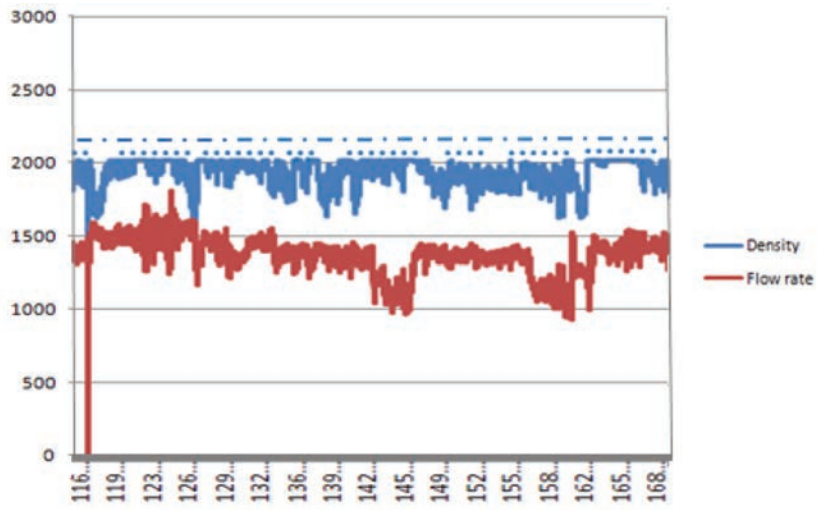


Figure 37. Recorded and expected froth pump performance

the 90 kW motor was more than sufficient for the duty. It was further noted that even with the 5% additional power requirement for the expeller seal configuration, the total motor absorbed kilowatt calculations indicated that the 4E-AHF™ froth pump was absorbing merely 45% to 60% of installed motor capacity, compared with the higher kilowatt absorbed calculations for the smaller 3CC-AHF™ froth pump.

After six months of trouble-free operations, a process fault contributed to the automatic isolation of the suction valve while the 4E-AHF™ froth pump was operational. The valve fault resulted in some damage to the volute, back liner, and Hi Seal® expeller.

After the six-month operation period and being subjected to adverse dry running conditions, the 4E-AHF™ froth pump impeller was found to be in a very good condition. Figure 38 shows the condition of the impeller removed from the pump. Only very limited wear could be observed around the inducer impeller vane tips, and this is attributed mainly to the dry run conditions.

Figure 39 shows the impeller reinstalled after the damaged components had been replaced.

After the repair, the froth pump was returned to full service with no further complications being reported. The 4E-AHF™ froth pump ran well for a further seven months, demonstrating extended periods of underflow pumping at densities above 1990 kg/m^3.

Just short of fourteen operational months, the SCADA recordings showed a rapid decline in pumping performance. The pump was stopped and disassembled, and it was found that the froth pump impeller and throat bush liner had reached their life expectancy (Figure 40).

Apart from outperforming the pumping capabilities of the conventional slurry pump, the 4E-AHF™ froth pump outlasted the conventional slurry pump by factor greater than two.



Figure 38. Froth pump impeller after six months service



Figure 39. The impeller reinstalled



Figure 40. The froth pump impeller and throat bush liner at end of life

Conclusions

In detailed site test work undertaken on a phosphate concentrate thickener underflow application, the Warman® AHF™ froth pump demonstrated significant improvements in the pumping of viscous non-Newtonian slurries. The effect of viscous slurries on pump performance remains complex as the velocity gradients within the pump vary considerably. However, the large AHF™ froth pump suction inlet, coupled with the unique flow inducer open vane impeller, has conclusively demonstrated improved shearing capability in comparison to a conventional closed-vane slurry pump impeller design.

The improved slurry flow dynamics encountered when using the 4E-AHF™ froth pump have shown that sustainable pumping practice is possible at BEP duty positions well below 25%, with no side effects of cavitational or aggressive suction recirculation damage.

In the absence of any rheology test work, predicting the friction factors and slurry behaviour can easily contribute to incorrect pump sizing, speed selections, and motor requirements.

Site application testing has shown that determining optimum pump performance for pumping viscous or paste-like non-Newtonian slurries must be done in conjunction with rheology test work and direct measurements of pump performance.

Rheology test work indicated that the rheograms for the lower slurry densities demonstrated a yield dilatant (shear-thickening) behaviour, whereas the rheograms for the higher slurry densities demonstrated a yield pseudoplastic (shear-thinning) behavior. Changes in the site system curves could not be accurately estimated, but were assumed to be as a result of both the rheology and flow regime behavioural changes.

The complexity of the thickener 11 underflow slurry rheology could not have been properly analysed without conducting comprehensive rheology test work.

The AHF™ froth pump impeller inducer vanes greatly assist with drawing the high concentration slurries into the eye and vane passages. Based on wear life, it has been noted that with adequate shearing of the viscous slurries, the unique froth pump impeller design has the ability to transport slurries at high solids concentrations with a reduced erosional impact. As the viscous slurries are effectively transferred through the vane passages, the particles tend to interact, forming a cushioning layer over the impeller vanes. This has some influence on sliding abrasion, but the harmful wear pattern caused by turbulent particle impact is greatly reduced. Test results proved that the froth pump impeller outlasted the conventional slurry pump impeller by nearly three times. Contrary to what might have been expected, a reduction in head and kilowatt

adsorbed values was noted for the underflow slurry duties at higher densities compared to the lower density duties. This was a result of higher densities at lower head losses coupled with the shear-thinning behaviour and the nature of flow within the froth pump.

In addition to the 4E-AHF™ froth pump being able to sustain the underflow slurry transfer at densities well above 1950 kg/m^3, the dry Hi Seal® expeller design complements effective gland sealing, thus offering zero dilution of the pumped medium.

The overall benefit of the more stable dense underflow slurry stream feeding the belt filter is the substantially reduced moisture content to the filter belt, with significant reductions in operational costs associated with spillage and dewatering operations.

From this thickener underflow case study, it is evident that the Warman® AHF™ froth pump design significantly outperforms the conventional slurry pump. The client has subsequently ordered more AHF™ froth pumps for retrofitting on two more concentrate thickener underflow applications.

Acknowledgements

To John Otten of Weir Minerals Division, JD Singleton, and Murray Jooste of Weir Minerals Africa for their technical assistance.

To Louw Botha and Shadrack Baloyi of Foskor for the opportunity and collaboration during the thickener underflow tests.

References

BURGESS, K.E. 2004. Developments in the pumping of mineral froths and non-Newtonian slurries. Warman Pump Technology Centre, Sydney. pp. 1–12.

LOZHECHNIKOVA, A. 2011. Determination of slurry's viscosity using case based reasoning approach. Master's thesis, Faculty of Technology, Lappeeranta University of Technology, Finland. pp. 9–15.

PATERSON, A. and COOKE, R. 2009. The design of slurry pipeline systems. Short course. Paterson & Cooke, Claremont.

TAYLOR, W.R. 2013. A new froth pump for improved flotation concentration handling. *Seventh Southern African Base Metals Conference*, Ingwenyama Conference & Sports Resort, Mpumalanga, South Africa, 2–4 September 2013. Symposium Series S76. Southern African Institute of Mining and Metallurgy, Johannesburg. pp. 115–138

TheFreeDictionary.com. 2014. Coefficient of rigidity., from The Free Dictionary: Dictionary, Encyclopedia and Thesaurus: http://encyclopedia2.thefreedictionary.com/coefficient+of+rigidity [Accessed 8 May 2014].

VIETTI, A.V. 2014. Slurry dewatering and thickener operation. Short course. Paterson & Cooke, Johannesburg.

WEIR MINERALS AFRICA. 2010. AH™ Upgrade Project - Improved dry gland expeller sealing. *Technical Bulletin no. 7 - Version* . pp 1–4.

WEIR MINERALS AFRICA. 2009. Pumping non-Newtonian slurries. *Technical Bulletin no. 14 - Version 2*. pp. 1–4.

WILLS, B. 2006. An introduction to the practical aspects of ore treatment and mineral recovery. *Mineral Processing Technology*. Elsevier, Oxford. pp. 382–385.

WILSON, K.C., ADDIE, G.R., SELLGREN, A., and CLIFT, R. 2006. Slurry Transport using Centrifugal Pumps. 3rd edn. Springer, New York.



Warren Richard Taylor

Product Specialist, Weir Minerals Africa (Pty) Ltd

Since 1993, I have been involved in supplying mining and mineral processing equipment to the heavy industrial and mining sectors.

Between 2001 and 2005, I managed a branch for a fan company, and was involved with designing and supplying air purification and materials handling equipment to processing plants.

Between 2005 and 2007, I headed up a branch specialising in bearing reclamation work and analysing bearing failures on mineral processing equipment.

In 2007, I joined Weir Minerals Africa, and since then have been extensively involved in supplying mineral processing solutions and optimisation programs to beneficiation plants in South Africa and West Africa.

As economic drivers continue to encourage innovation, technological change is inevitable. Introducing new centrifugal pumping technology to the mineral processing industry remains my primary objective by presenting end-users with comprehensive optimisation programs and process improvement solutions based on detailed application engineering modelling.

Highlights of the most recent process improvements and optimisation programs completed by myself, assisted by my colleagues, are as follows:

- *2011 Upgrading of the process water and water recovery system for a large flotation and filtration plant:* This optimisation program involved installing, commissioning and testing the cutting-edge Warman DWU dewatering 7000 kPa high lift dirty water pump technology – first DWU installation in the world.
- *2012 Upgrading of a large residue disposal system to a TSF:* This optimisation program involved supplying, commissioning and testing the latest high pressure Warman slurry pump technology for a new 6-stage 14/12-AHPP 6900 kPa tailings disposal system, whereby all pump-sets were directly driven by medium voltage 530kW 10Pole motors – first installation of this design in South Africa.
- *2012 Upgrading of the froth transfer systems for a flotation plant:* This optimisation program involved designing, supplying, commissioning and testing the ultra-modern Warman AHF froth pump and froth hopper technology for a phosphate flotation plant – first installation of this design in South Africa.

From the 2012 froth transfer optimisation program, a case study article based on the successful implementation of the new AHF froth pumping technology was written and published by the SAIMM (presented at the 2013 Base Metals Conference).

This 2014 article will be my second article for publication by the SAIMM, and focuses on a thickener underflow process improvement for pumping viscous non-Newtonian slurries using the same AHF froth pumping technology.